Title
Landmark-free geometric methods in biological shape analysis

Permalink
https://escholarship.org/uc/item/5kk16831

Journal
Journal of The Royal Society Interface, 12(113)

ISSN
1742-5689

Authors
Koehl, Patrice
Hass, Joel

Publication Date
2015-12-01

DOI
10.1098/rsif.2015.0795

Peer reviewed

Author for correspondence:
Patrice Koehl
e-mail: koehl@cs.ucdavis.edu

THE ROYAL SOCIETY
PUBLISHING

Landmark-free geometric methods in biological shape analysis

Patrice Koehl[1] and Joel Hass[2]

[1]Department of Computer Science and Genome Center, and [2]Department of Mathematics,
University of California Davis, Davis, CA 95616, USA

In this paper, we propose a new approach for computing a distance between two shapes embedded in three-dimensional space. We take as input a pair of triangulated genus zero surfaces that are topologically equivalent to spheres with no holes or handles, and construct a discrete conformal map f between the surfaces. The conformal map is chosen to minimize a symmetric deformation energy $E_{sd}(f)$ which we introduce. This measures the distance of f from an isometry, i.e. a non-distorting correspondence. We show that the energy of the minimizing map gives a well-behaved metric on the space of genus zero surfaces. In contrast to most methods in this field, our approach does not rely on any assignment of landmarks on the two surfaces. We illustrate applications of our approach to geometric morphometrics using three datasets representing the bones and teeth of primates. Experiments on these datasets show that our approach performs remarkably well both in shape recognition and in identifying evolutionary patterns, with success rates similar to, and in some cases better than, those obtained by expert observers.

1. Introduction

Geometry and topology have had increasing impact in biology over the last two decades. The application of mathematical methods in biological studies has not only become viable but in fact is assuming a central role, owing to the increasing performance of computers and the improvement of the devices used for imaging biological systems. In medicine, for example, diagnosis and treatment planning previously relied on conventional X-ray images, recorded on an analogue film. Today, however, more and more digital three-dimensional images, such as those generated with computed tomography, magnetic resonance imaging, and functional, marker-based images are acquired from patients to detect and monitor putative pathologies. This has driven the need for software development to analyse those images, which in turn has provided a major impetus for the development of new mathematical methods and algorithms for image processing. With these new software tools, the three-dimensional images can be quantitatively analysed and visualized, making medical diagnosis, the assessment of therapeutic strategies, and even surgery more reliable and reproducible [1].

The comparison of images and of the shapes they represent is by no means limited to medicine. Advances in geometry and topology, and the parallel transformation of biology into a quantitative science, have led to a renewed interest in applying geometric methods to representing, searching, simulating, analysing and comparing biological systems [2]. These methods are developed and applied in a wide range of fields, including computer vision, biological imaging, brain mapping, target recognition and for satellite image analysis. In molecular biology, the notion that the structure (or shape) of a protein is a major determinant of its function has led to the development of methods for representing, measuring and comparing protein structures [3–5]. Brain morphometry, concerned with the measurement of the brain geometric structures and the changes they undergo during development, ageing, learning, disease and evolution, has become central in neurobiology [6–10]. Morphometrics, the quantitative analysis of forms, has equal potential in evolutionary biology [11–14], though its impact in this field has been somewhat obscured by the

phenomenal success of molecular phylogenetics [15]. There is hope however that information from both approaches can be combined to reach a synthetic, comprehensive and quantitative view of phylogeny (see, for example, [16,17] for successful integration in the field of palaeoanthropology). To reach this goal, geometric morphological studies need to be automated and standardized, starting with the determination of geometric correspondence between shapes [14,18]. This paper concerns mathematical and computational aspects of this problem.

While three-dimensional data representing a shape come in many forms, we concentrate on the important and commonly occurring case where the surface of the shape is available and described with a discrete triangular mesh. Thus, we are interested in understanding the structure of surfaces situated in our three-dimensional world. Mathematically, these objects are two-dimensional Riemannian manifolds in the smooth case, and piecewise-flat surfaces in the discrete setting. We work with both descriptions. We restrict ourselves to surfaces of genus zero. These are the surfaces that can be continuously deformed to a sphere, or, alternatively, surfaces that have no holes or handles.

In a chapter titled 'The comparison of related forms', Thompson [19] explored how differences in the forms of related animals can be described by means of simple mathematical transformations. This inspired the development of several shape comparison techniques whose aim is to define a map between two shapes that can be used to measure their similarity. This is a challenging problem, as the space of possible maps is extremely large and difficult to characterize mathematically. In this paper, we develop methods that generate maps between two shapes corresponding to surfaces of genus zero.

The dimension of the space of maps between two shapes can be reduced by enforcing correspondence between specific landmarks. Ideally, these landmark points should identify homologous structures on the surfaces of the two shapes, should conserve their relative positions, should provide adequate coverage and should be found reliably and consistently [2]. The task of finding such landmark points is usually performed manually by skilled morphometricians with extensive training. The resulting human choices can lead to error due to the variability and inconsistency of human input [20]. Many methods have been developed to circumvent this inherent limitation, either through automation of the landmark selection process or by eliminating the need to use specific point correspondence in the process of aligning the surface altogether. Automatically selected points may relate to distinctive geometric features such as local curvature maxima [21], be inferred from an atlas for the shape of interest [22], or be optimally distributed on the surface of interest based on some statistical criteria [23,24]. Spectral techniques, for example, assign a signature to each vertex in the mesh, under the premise that points with similar signatures are more likely to correspond [25,26]. There is a growing interest in the concept of semi-landmarks. These are points that characterize the outlines of the shapes of interests. The positions of these points are optimized to match the positions of corresponding points along an outline in a reference conformation [12,27–31]. Despite the optimization procedures, there is no guarantee that these points are placed accurately and consistently across collections of surfaces, unless those surfaces are highly homologous. In addition, most of the techniques based on semi-landmarks for three-dimensional shapes still rely on a few user-defined

landmarks [29,32]; as such, they do not fully remove the inherent limitation of the variability of human input. Landmark-based methods that find maps between two shapes work on the premise that knowledge of a mapping on a small number of correspondences can be extended to give the full map between the two surfaces of interest [33–35]. By contrast, landmark-free methods skip the search for landmarks altogether. For example, Valliant & Glaunès [36] introduced a representation of surface in the form of currents and then imposed a Hilbert space structure on it, whose norm is used to quantify the similarity between two surfaces. McCane [37] developed a variational method for matching curves in two or three dimensions by optimizing their parametrizations. In parallel, Laga *et al.* [38] developed statistical models of shapes based on the squared root velocity function that allow for the modelling of shape variability without considering landmarks. They recently implemented this procedure to study the shapes of plant leaves [38].

In a groundbreaking recent paper, Boyer *et al.* [13] introduced several distance measures that can be used to generate fully automated correspondences between surfaces. They tested their approaches on three datasets representing the skeletal anatomy of a collection of primates, showing success in taxonomic classifications [13]. These approaches were tailored to topological discs, as all the datasets represent surfaces having the topology of a disc. That is, the surfaces can be obtained from a flat disc in the plane by stretching and bending, but without tearing or gluing. We present here a new algorithm that has a similar philosophy to their work, but uses a very different geometric distance measure. As with their method, our approach fully eliminates the use of landmarks. While they measured distortion based on area-preserving maps with a continuous Procrustes distance and general maps with a Wasserstein distance, we work entirely within the framework of conformal (angle-preserving) maps and focus on finding a *globally optimal conformal mapping* between two genus zero closed surfaces. We associate an energy to any conformal map between two such surfaces. We show that the energy of the optimal map defines a metric on the space of surfaces of genus zero. Experiments on the same datasets as those used by Boyer *et al.* [13] show that our method outperforms their distance measures in identifying evolutionary patterns between the specimens whose bones are included in the datasets and, indeed, performs as well as or better than trained observers. We note that while our algorithm was developed to compare spherical or genus zero surfaces, it can also be used to compare disc-like surfaces. To do so, we introduce a preliminary step where the holes of a surface are filled in (coned) to create a closed surface. We expect that our method would perform even better in studies where the compared surfaces were already of genus zero.

This paper develops previous preliminary studies [39,40]. We have modified the elastic energy used to measure the distance of an optimal conformal mapping from an isometry so that it now defines a mathematical metric on the space of shapes. The paper is organized as follows. Section 2 provides the mathematical background for our method: conformal geometry and a metric to measure the similarity between surfaces of genus zero. The details of its implementation on discrete surfaces are provided in the electronic supplementary material. Section 3 presents and discusses the results obtained by our algorithm on three test cases introduced by Boyer *et al.* [13]. We conclude the paper with a brief discussion on the

implications of this work on using phenetics to reconstruct phylogeny, and on future developments of the method itself.

2. A new distance between shapes

2.1. Optimal conformal map between genus zero surfaces

Let F_1 and F_2 be two surfaces of genus zero and equal area. By rescaling each surface, it is straightforward to arrange for all surface areas to be equal to 1. While our method allows us to compare surfaces of different areas, we focus here on scale invariant shape properties. A map f from F_1 to F_2 defines for each point $z \in F_1$ a corresponding point $f(z) \in F_2$, called the image of z under f. For smooth surfaces, one can specify the angles between two curves. Maps that preserve these angles are called conformal. Such maps do not need to preserve length. Examples of conformal maps include the Mercator projection used in cartography and the stereographic projection that maps a sphere (minus its North Pole) onto the plane.

A conformal map preserves angles but usually distorts distances, with isometries being the exception. This distortion is characterized by a *dilation* factor, $\lambda_f(z)$, that measures the stretching of vectors by f at each point z in F_1. This stretching is the same in all directions.

Our objective is to find a conformal map between the two genus zero surfaces F_1 and F_2 that is as close to an isometry as possible. An isometry has two distinct local properties. It preserves angles at each point (conformality) and it preserves area. There is a natural choice for picking a map that is as close to an isometry as possible. One first restricts to finding a conformal map between the two surfaces. The uniformization theorem ensures the existence of such a map, and indeed of many such maps between any two surfaces of genus zero [41]. To pick the best conformal map, it is natural to use the second criterion of an isometry, area preservation, and choose a conformal map that minimizes the local area distortion. This is the underlying idea of our method, as described in [39,40,42].

Following this idea, the conformal map f between F_1 and F_2 can be described as the composition of three conformal maps, $C_1 : F_1 \to S^2$, $m : S^2 \to S^2$ and $C_2^{-1} : S^2 \to F_2$. The map m is an element of the six-dimensional group PSL(2, C) that describes all conformal maps from the round sphere S^2 to itself. Figure 1a illustrates this process for two proximal metatarsal bones of primates.

Varying m gives all conformal maps from F_1 to F_2. We specify the optimal m to be the one that leads to a minimum of the following symmetric distortion energy integral energy E_{sd}:

$$E_{sd}(f) = \sqrt{\int_{F_1} (1 - \lambda_f(z))^2 dA_1}$$
$$+ \sqrt{\int_{F_2} (1 - \lambda_{f^{-1}}(z))^2 dA_2}. \quad (2.1)$$

A conformal map f is an isometry if and only if its dilation $\lambda_f(z)$ at every point z is equal to 1. $E_{sd}(f)$ is the natural measure of how $\lambda_f(z)$ and $\lambda_{f^{-1}}(z)$ differ from 1, and therefore of how f and f^{-1} deviate from an isometry. Note that $E_{sd}(f) = E_{sd}(f^{-1})$. The infimum of the magnitude of $E_{sd}(f)$ as f varies over all conformal

diffeomorphisms from F_1 to F_2 exists [42] and is used to define the distance between the two surfaces.

The symmetric distortion energy defined in equation (2.1) has the following properties [42]:

(1) for any pair of genus zero surfaces, there exists a smooth conformal diffeomorphism f_{min} between them that minimizes the symmetric distortion energy,
(2) the symmetric distortion energy of a map is zero if and only if the map is an isometry,
(3) the symmetric distortion energy of f_{min} defines a metric d_{sd} on the space of genus zero surfaces, so that d_{sd} satisfies the following three properties, (i) $d_{sd}(F_1, F_2) \geq 0$, with equality if and only if F_1 and F_2 are isometric, (ii) $d_{sd}(F_1, F_2) = d_{sd}(F_2, F_1)$, and (iii) $d_{sd}(F_1, F_3) \leq d_{sd}(F_1, F_2) + d_{sd}(F_2, F_3)$.

Property (iii) of the metric d_{sd}, the triangle inequality, is important for applications, as it implies robustness. Namely, if the distances $d_{sd}(F_1, F_1')$ and $d_{sd}(F_2, F_2')$ are small, this property guarantees that $d_{sd}(F_1, F_2)$ is close to $d_{sd}(F_1', F_2')$. Thus, the distance measure is stable under noise and measurement errors.

2.2. Comparing discrete genus zero surfaces

In practice, the two surfaces F_1 and F_2 are discrete and represented by meshes $\mathcal{M}_1$ and $\mathcal{M}_2$, respectively. Meshes are taken to be triangular, so that $\mathcal{M}_i = (V_i, E_i, T_i), i = 1, 2$, where $\{V_i, E_i, T_i\}$ denote the vertices, edges and faces, respectively. We do not restrict the topologies of the meshes to be the same. The number of vertices, edges and faces of $\mathcal{M}_1$ and $\mathcal{M}_2$ can be different. The method described above for computing an optimal conformal map between two smooth surfaces needs to be adapted for its applications to their discrete counterparts. While we refer the reader to our previous papers [39,40] and to the electronic supplementary material for a full description of this adaptation, we summarize here the changes that are relevant to this paper.
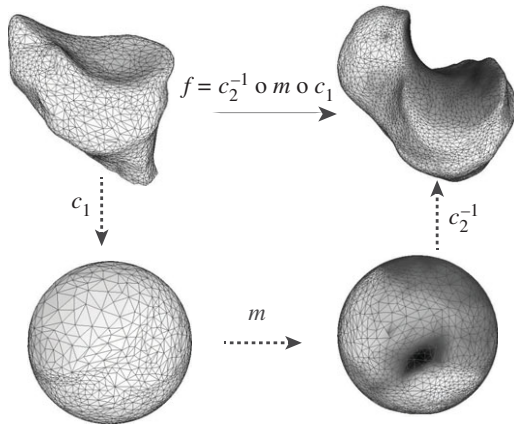
The total distortion for a mesh is a discrete version of the symmetric distortion energy given by equation (2.1) and is computed as a sum over all edges of the two surface meshes

$$E_{sd}(f) = \sqrt{\sum_{(v_i, v_j) \in E_1} \left(1 - \frac{l(f(v_i), f(v_j))}{l(v_i, v_j)}\right)^2 \frac{A_{ij}}{3}}$$
$$+ \sqrt{\sum_{(v_m, v_n) \in E_2} \left(1 - \frac{l(f^{-1}(v_m), f^{-1}(v_n))}{l(v_m, v_n)}\right)^2 \frac{A_{mn}}{3}}. \quad (2.2)$$
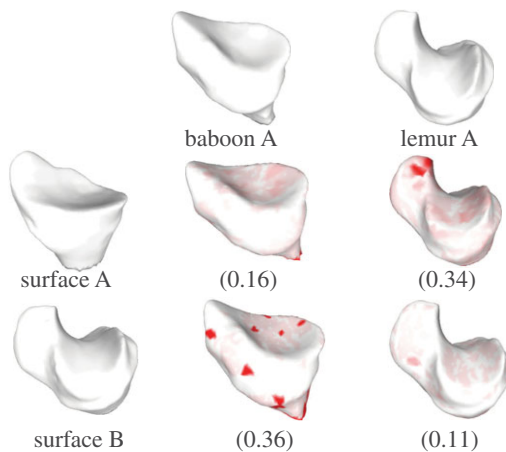
Here E_1 and E_2 denote the sets of edges in the meshes on F_1 and F_2, respectively. A_{ij} is the sum of the areas of the two triangles adjacent to the edge v_i, v_j and $l(v_i, v_j)$ is the distance between the two vertices v_i and v_j, namely the length of the edge (v_i, v_j).

The image $f(v)$ of a vertex v of the mesh $\mathcal{M}_1$ is not artificially restricted to correspond to a vertex of the mesh $\mathcal{M}_2$. Instead, v is mapped to an arbitrary point belonging to one face of $\mathcal{M}_2$. Special care is then needed for computing distances. The distance between two vertices v_i, v_j forming an edge e_{ij} of F_1 is simply the length of this edge. The images $f(v_i)$ and $f(v_j)$ most likely do not form an edge of F_2. The distance $l(f(v_i), f(v_j))$ is computed using a flat Euclidean metric on each face of the triangulation. Figure 1b illustrates the calculation of $E_{sd}(f)$ on two edges.
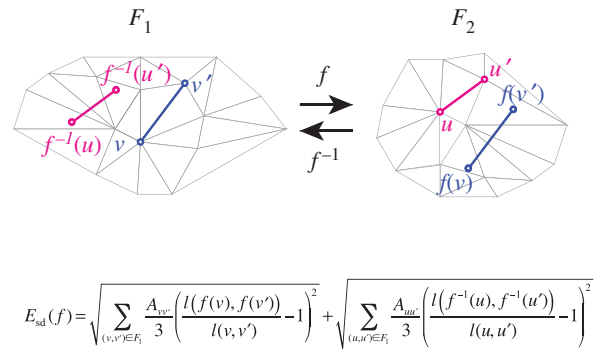
(*a*) building a conformal map

$$f = c_2^{-1} \circ m \circ c_1$$

c_1 c_2^{-1}

m

(*b*) optimizing the conformal map

F_1 F_2

$f^{-1}(u')$ v' u' $f(v')$

f u

$f^{-1}(u)$ v f^{-1} $f(v)$

$$E_{sd}(f) = \sqrt{\sum_{(v,v') \in F_1} \frac{A_{vv'}}{3}\left(\frac{l(f(v), f(v'))}{l(v, v')} - 1\right)^2} + \sqrt{\sum_{(u,u') \in F_1} \frac{A_{uu'}}{3}\left(\frac{l(f^{-1}(u), f^{-1}(u'))}{l(u, u')} - 1\right)^2}$$

(*c*) shape recognition and classification

baboon A   lemur A

surface A   (0.16)   (0.34)

surface B   (0.36)   (0.11)

(*d*) evolutionary tree derived from geometric distances
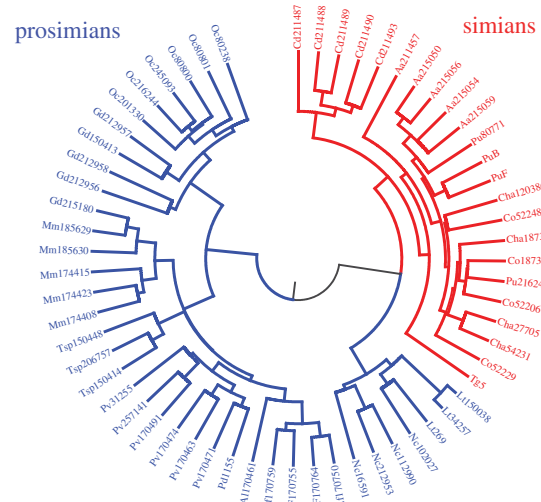
prosimians   simians

Figure 1. An optimal conformal map and its applications. (*a*) The comparison of two surfaces F_1 and F_2 relies on the existence of a map f between these surfaces. When the two surfaces are of genus zero, it is possible to construct f as a composition of three maps C_1, m and C_2, where C_1 and C_2 are conformal maps from the surfaces F_1 and F_2 to the sphere and m is a bijective conformal map of the sphere to itself. The key to our approach is that the group of conformal self-maps of the sphere is the well-understood group of Möbius transformations. As such, m is defined by six parameters that can be optimized to yield minimal distortion. (*b*) Distortion is computed as the sum of the stretching induced by f on all edges (v, v') in the mesh describing F_1, and of the stretching induced by f^{-1} on all edges (u, u') in the mesh describing F_2. In the corresponding symmetric distortion energy $E_{sd}(f)$, each edge is weighted by the areas of its adjacent triangles. The energy of the minimizing map defines a distance d_{sd} on the space of surfaces of genus 0. (*c*) Shape recognition is a natural application for the method described here. All surfaces shown here correspond to proximal metatarsal bones from baboons and lemurs. When the surface A is mapped onto the surfaces for baboon A and lemur A, the corresponding symmetric distortion distances d_{sd} are 0.16 and 0.34, respectively, identifying surface A as corresponding to a baboon. By contrast, surface B is closer to lemur A, and therefore corresponds to a lemur. Regions on the images with large stretching are coloured. (*d*) The unweighted pair group method with arithmetic mean (UPGMA) tree built from the distance matrix computed from a comprehensive comparison of all bones in database A clearly separates those bones into two categories, those from prosimians (left) and those from simians (right). This geometry-based categorization of the primates obtained from the metatarsal shapes can then be combined with other classifications to help understand their phylogeny. (Online version in colour.)
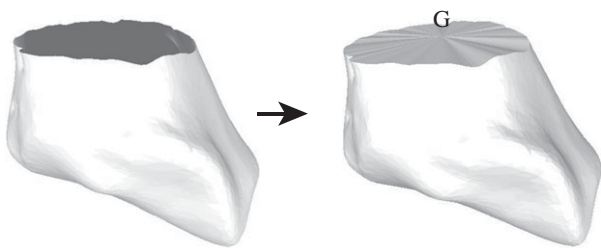

G

Figure 2. Coning off a surface with boundary. The method presented in this paper is currently optimized for surfaces of genus zero. These surfaces do not have a boundary. The meshes included in our test sets however have one boundary, whose limits are somewhat arbitrary. To fill in the corresponding hole, we detect all vertices and edges on the boundary, compute the centre of gravity G of these vertices, and add to the mesh all the triangles formed by connecting G to the edges of the boundary. The result is a genus zero surface with no boundary.

We have implemented this procedure into the program MatchSurface. A complete description of its algorithms is given in the electronic supplementary material. For a pair of surfaces F_1 and F_2 represented by meshes $\mathcal{M}_1$ and $\mathcal{M}_2$, MatchSurface produces an approximation for the map f_{min} that minimizes the symmetric distortion energy E_{sd} over all conformal maps between F_1 and F_2. Its output consists of the image $W_m(\mathcal{M}_1)$ of $\mathcal{M}_1$ warped by f_{min} onto F_2, the image $W_m^{-1}(\mathcal{M}_2)$ of $\mathcal{M}_2$ warped by f_{min}^{-1} onto F_1, and the distance $d_{sd}(F_1, F_2) = E_{sd}(f_{min})$. Applications of MatchSurface include, but are not limited to, (i) comparing a surface F_U of unknown origin with a library of surfaces that are well characterized, using the best matching surface as a template to infer properties for F_U (figure 1*c*) and (ii) construction of a neighbour joining tree that captures the hierarchical geometric similarities between a set of surfaces. This tree can then be related to

Table 1. Correlations between observer distances, cP and sd distances.

dataset	no. pairs	obs1/cP	obs2/cP	obs1/sd	obs2/sd	obs1/obs2
metatarsal (all)	1830	0.62	0.63	0.82	0.81	0.87
metatarsal (same species)	112	0.31	0.17	0.55	0.31	0.46
metatarsal (different species)	1718	0.57	0.58	0.79	0.78	0.85
radius (all)	990	0.28	n.a.	0.59	n.a.	n.a.
radius (same species)	198	0.29	n.a.	0.40	n.a.	n.a.
radius (different species)	792	0.13	n.a.	0.46	n.a.	n.a.
teeth (all)	4851	0.55	n.a.	0.58	n.a.	n.a.
teeth (same genus)	180	0.01	n.a.	0.63	n.a.	n.a.
teeth (different genus)	4671	0.51	n.a.	0.51	n.a.	n.a.

properties of the objects it represents, such as phylogeny, as illustrated in figure 1*d*.

3. Results

To test the effectiveness of MatchSurface, we applied it on three independent datasets, representing three regions of the skeletal anatomy of a collection of primates. The first dataset contains 61 proximal first metatarsals of prosimian primates, New and Old World monkeys, the second dataset contains 45 distal radii of apes and humans and the third dataset includes 116 second mandibular molars of prosimian primates and non-primate close relatives. They were originally assembled by Boyer *et al.* [13], who used them in a similar study with different shape comparison measures based on an 'earth mover' metric, and on a 'continuous Procrustes' (cP) distance. We note that all meshes included in the three datasets represent genus zero surfaces with one boundary. The position of this boundary is somewhat arbitrary. Its impact on the study by Boyer *et al.* was not discussed. Similarly, it will not be considered here. We did however detect and clean up those boundaries by removing 'dangling' triangles, i.e. triangles with two boundary edges (see the electronic supplementary material for details). Our method is designed for genus zero closed surfaces. It easily extends however to genus zero surfaces with boundaries by coning off the boundary curves (see figure 2 for an illustration of this process). Using these datasets allows us to evaluate the performances of the algorithm implemented in MatchSurface. The evaluation is done by comparing the distances d_{sd} between the surfaces included in the three datasets with the continuous Procrustes distances provided by Boyer *et al.*, and with the distances based on landmarks identified by trained morphologists. The datasets include two sets of the latter for the metatarsal dataset, referred to as 'observer1' (obs1) and 'observer2' (obs2), and one set for the radii dataset and the teeth dataset, 'observer1'. We note that the cP distance, in common with d_{sd}, does not require preliminary selection of landmarks on the surfaces. Geometric morphometricians on the other hand have determined landmarks on each surface, choosing them to reflect correspondences considered biologically and evolutionarily meaningful (see SI Appendix, Materials of [13]). These landmarks determine a 'discrete' Procrustes distance between any two surfaces, which we refer to as d_{obs}. Each of the three distances (d_{sd}, d_{cP} and d_{obs}) defines a matrix for each dataset,

containing all pairwise distances between the surfaces included in that dataset. To measure the effectiveness of each distance, we compare those matrices in three different ways.

All three distances rank pairs of surfaces according to their similarity. The relative performance of d_{sd} and d_{cP} with respect to the observer distance d_{obs} can then be computed using a correlation analysis. Table 1 gives the corresponding coefficients.

The distances based on manual assignments of landmarks by morphometricians may be considered as a reference, since they are based on extensive expert knowledge, though they are not deemed perfect. Note that there is variability between morphometricians, though the correlations between the results of two such observers is high. On all three datasets, the distances based on sd match observer distances better than the distances based on cP.

This advantage is further illustrated in figure 3.

The match between d_{sd} and the observer distance d_{obs} is more consistent over the whole range of values. We note that all three distances identify the pairs of surfaces corresponding to specimens from the same species as being similar (red circles in figure 3). Even on this subset of all pairs, however, d_{sd} is better correlated to the observer distances (table 1). The same behaviour is observed for pairs of surfaces from specimens that belong to the same family or to the same superfamily (results not shown). Note that the similarities found between the d_{sd} distances and the observer distances are comparable to those between the two observers.

For a second comparison of the three distance measures, we evaluated their performance using a receiver operating characteristic (ROC) analysis [43]. In this approach, a 'gold standard' is defined, based on a choice of level in the phylogeny of the specimens, either species, genus, family or superfamily. A pair of surfaces is then defined as similar, or 'positive', if the corresponding specimens belong to the same taxonomic group considered, and 'negative' otherwise. For varying thresholds of the distance measure under study, all pairs of surfaces whose distances fall below the threshold are then assumed positive, while those above it are deemed negative. The pairs that agree with the standard are called true positives (TPs), while those that do not are false positives (FPs). An ROC analysis compares the rate of TPs (also called sensitivity) to the rate of FPs (which corresponds to 1 minus the sensitivity). It is scored with the proportion of area under the corresponding curve (AUC). An AUC of 1 indicates that all TPs are detected first. This corresponds to the ideal distance measure. On the other hand, the diagonal curve leads to an AUC of 0.5.
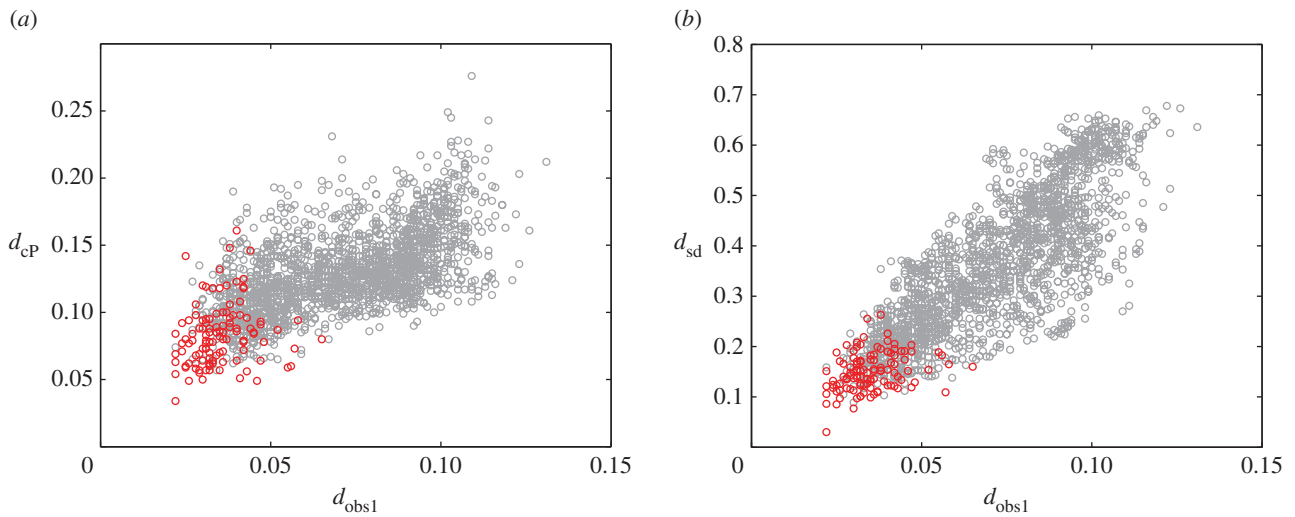
Figure 3. Comparison of the observer distance with the cP distance (*a*), and the sd distance (*b*). Results are shown for the metatarsal database. Red circles correspond to pairs of surfaces from specimens that belong to the same species. The distances between same species pairs are expected to be small for any of the three distance measures. This is indeed the case, as the corresponding points are found to cluster in the lower left corner of the plots. The correlation coefficients between d_{cP} and d_{obs1} and between d_{sd} and d_{obs1} over all pairs of surfaces are 0.62 and 0.82, indicating that d_{sd} matches better with the observer1 distance, over a broader range or values. We also compute the ratio of the range of distance values for the pairs corresponding to specimens from the same species over the range of values for all pairs of surfaces in the dataset. A lower ratio indicates better performance, as a large ratio would indicate lower discrimination of the significant pairs. We find ratios of 50%, 39% and 36% for the cP distance, the observer1 distance, and the sd distance, respectively.

Table 2. Area under the curve (AUC) of ROC analyses on the observer, cP and sd distances.

dataset classification	first metatarsal					radius				teeth			
	N	obs1	obs2	cP	sd	N	obs	cP	sd	N	obs	cP	sd
species	13	0.94	0.97	0.90	0.96	5	0.87	0.72	0.87	n.a.	n.a.	n.a.	n.a.
genera	13	0.94	0.97	0.90	0.96	4	0.86	0.71	0.80	24	0.98	0.96	0.97
families	9	0.91	0.95	0.84	0.95	n.a.	n.a.	n.a.	n.a.	17	0.87	0.79	0.86
superfamilies	2	0.96	0.97	0.73	0.86	n.a.	n.a.	n.a.	n.a.	5	0.64	0.62	0.77

In this case, TP and FP appear at the same rate, and the distance measure contains no information.

The results of ROC analyses based on the three distances d_{sd}, d_{cP} and d_{obs} are given in table 2 and illustrated in figure 4.

Species or genera identification based on landmarks manually defined by experts is expected to perform best. Indeed, the ROC curves derived from the observer distances illustrate excellent classification results, with AUC values above 0.85 in all cases, above 0.9 for the metatarsal dataset, and above 0.95 for the teeth dataset. Note that even with human expertise included, the classification is not perfect. In addition, we observe differences between the results obtained by two distinct experts. The two distance measures d_{cP} and d_{sd} alleviate the difficulty of defining landmarks on the two surfaces to be compared. Instead, both methods construct a map between the two surfaces using only their geometric properties. The distances they compute reflect different geometric properties. We find that the distance d_{sd} introduced in this study outperforms d_{cP} on all three datasets, at all phylogenetic classification levels. In fact, d_{sd} performs as well as the observer, landmark-based distances, with differences that are of similar magnitude to the differences measured between distinct observers.

In such an ROC analysis, it is worth focusing on the small distances, as those are often the most reliable ones and the most relevant for applications. For each distance measure, we defined S_{200} to be the set of 200 pairs of surfaces with the lowest distances. Each pair was deemed to be 'true' or 'false' if the corresponding pair of specimens belonged to the same species or not, respectively. Table 3 reports the repartition of true and false pairs within S_{200} for the three distances considered here, for the three datasets. The higher the number of true pairs, the better. The rankings provided by d_{sd} are similar to those provided by the expert observers, outperforming the cP distance on all three datasets.

The ROC analysis ranks distances between specimens and assesses if this ranking is compatible with an existing classification; it does not perform the classification itself. We extend the ROC analysis to the actual problem of classification by performing a third set of computational experiments. Each experiment involves a dataset of surfaces/specimens, D, a taxon, T, and a distance measure, d. We begin by randomly dividing the sets of surfaces in D into two groups of approximately equal size. The first group serves as a training set to define the taxa, while the second group serves as a test set. A test surface is classified by assigning it to the taxon of its nearest neighbour in the training set. This is much akin to the 'threading' method illustrated in figure 1*c* and used in the protein structure prediction community [44]. The results
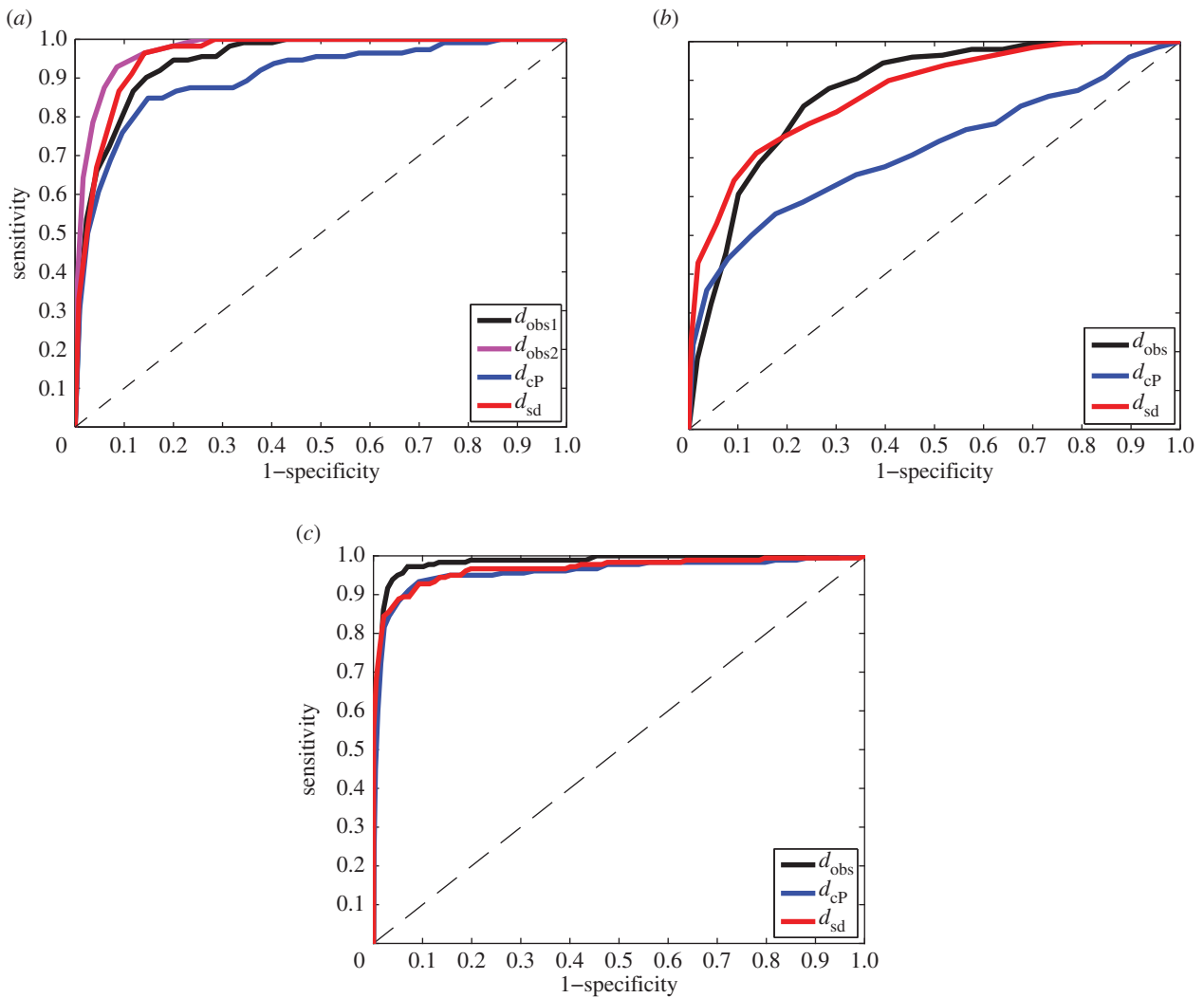
Figure 4. ROC analyses of three distance measures of surface similarities. We compare the effectiveness of an observer-based distance, d_{obs}, a continuous Procrustes distance, d_{cP}, and a symmetric distortion distance, d_{sd}, to detect similarities that identify with membership of the same species in a set of 61 metatarsal surfaces (a), in a set of 45 radius surfaces (b), and with genera in a set of 99 teeth surfaces (c). 'True' relationships are defined by the phylogeny of the specimens included in those datasets. An ROC curve that falls close to the first diagonal (shown as a dashed line) reveals poor performance, while an ROC curve that first follows the y-axis, i.e. whose area under the curve is the largest, indicates good performance. The results indicate that d_{sd} outperforms d_{cP} and is comparable to an observer-based distance.

Table 3. Repartition of the 200 smallest distances for the observer, cP and sd distances.

dataset distance	first metatarsal		radius		teeth	
	true (112)[a]	false (1718)	true (198)	false (792)	true (180)	false (4671)
observer1	81 (72%)	119 (7%)	120 (60%)	80 (10.1%)	134 (74.4%)	66 (1.4%)
observer2	98 (87.5%)	102 (5.9%)	n.a.	n.a.	n.a.	n.a.
d_{cP}	77 (68.7%)	123 (7.2%)	99 (50%)	101 (12.8%)	130 (72.2%)	70 (1.5%)
d_{sd}	86 (76.8%)	114 (6.6%)	127 (64%)	73 (9.2%)	138 (76.7%)	62 (1.3%)

[a]The distance between two surfaces is said to be true if the corresponding specimens belong to the same species, and false otherwise. The total number of such pairs is given in parenthesis. We chose the first 200 distances in both sets to guarantee that we would include both types of distances. We note that the best possible performance for a distance measure would find 112 true and 83 false distances for the metatarsal dataset, 198 true and 2 false for the radius dataset, and 180 true and 20 false for the teeth dataset.

are stored in a confusion matrix, C, whose element $C(i, j)$ reports the number of test surfaces corresponding to specimens that belong to taxon i that have been classified as belonging to taxon j. The accuracy of the classifier d is then defined to be the ratio of the trace of the confusion matrix over the sum of all its elements (i.e. the percentage of correctly classified specimens). To remove the influence of the initial division of the dataset into test and training sets, the procedure is repeated 5000 times. We performed these experiments for the three datasets, for the three distance measures and for different levels in the taxonomy of the specimens. The results are reported in table 4.

Table 4. Success rates of classification experiments, based on the observer, cP and sd distances.

dataset classification	first metatarsal					radius				teeth			
	N	obs1	obs2	cP	sd	N	obs	cP	sd	N	obs	cP	sd
species	13	74[a]	86	71	81	5	76	78	85	n.a.	n.a.	n.a.	n.a.
genera	13	74	86	71	81	4	85	85	90	24	87	87	94
families	9	83	94	82	93	n.a.	n.a.	n.a.	n.a.	17	91	89	93
superfamilies	2	100	100	98	100	n.a.	n.a.	n.a.	n.a.	5	94	95	95

[a]Percentage of correctly classified specimens, computed over 5000 experiments.

Classifications based on the sd distances outperform those based on the cP distances for the three anatomical datasets, and are similar in accuracy to those based on the observer distances, even outperforming them for the radius and teeth datasets. We note the significant differences between the two observers on the first metatarsal dataset. These differences indicate the difficulties in defining consistent landmarks on anatomical surfaces even for experienced morphometricians.

A distance matrix that contains the results of an all-against-all comparison of all specimens included in a dataset can be turned into a tree using a variety of clustering techniques. We used the unweighted pair group method with arithmetic mean (UPGMA) to build trees based on the four distance measures (d_{obs1}, d_{obs2}, and d_{sd}) for the first metatarsal dataset, as implemented in the software package PHYLIP [45]. UPGMA constructs a tree by minimizing the net disagreement between the matrix pairwise distances and the distances measured on the tree. Results are shown in figure 5. We note that those are phenetic trees, in opposition to phylogenetic trees that are built from molecular sequencing data.

The UPGMA tree based on d_{sd} shows a high level of agreement with the actual phylogeny of the specimens considered, both at the superfamily and at the family level. The two superfamilies, simians and prosimians, are clearly separated on the tree. In addition, nine clades with three or more branches only include specimens from the same family, with four of those exactly corresponding to one family, namely the Tarsiidae, Lemuridae, Lorisidae and Pitheciidae. We only observe one unusual association, namely the first metatarsal of one Galago is found to be very similar to the first metatarsal of a Cheirogaleidae, while other members of these two families are clearly distinguished. We note that similar, and sometimes larger, overlaps between these two families are observed in the phylogeny trees built from the observers' distances or from the cP distances. The tree based on observer1 distances shows even more misassociations, with members of the Lemuridae families (in green) being spread out over the Indridae and Cheirogaleidae families.

To quantify the differences between the trees generated from the observers, cP and sd distance matrices computed for the metatarsal dataset, we first rescaled those distance matrices so that all distances ranged between 0 and 1, and regenerated the UPGMA trees. The four trees are then compared using the TreeDist program from the software package PHYLIP. TreeDist computes the symmetric distance of Robinson & Foulds [47] to evaluate the similarity between two trees. We find that the distances between the observers' trees and the cP and sd trees are 96 and 84, and 86 and 82, respectively. While we cannot assess the meaning of the absolute values of these distances, and the significance of the differences between those values, we do notice that the observers' trees resemble most the tree computed with the sd method introduced here.

4. Discussion

Finding efficient algorithms to describe, measure and compare shapes is a central problem in numerous disciplines that generate extensive quantitative and visual information. Among these, biology occupies a central place. Structural biologists studying bio-molecular structures, neurobiologists studying the shapes of brain structures and their variations during ageing or in diseases, as well as morphometrists who use three-dimensional geometric morphometry are all concerned with characterizing three-dimensional shapes and computing distances between those shapes. In this context, we have developed a new method for automatically generating a conformal map between two surfaces of genus zero. This new approach leads to flexible registration of the two surfaces and accurate measurements of their geometric dissimilarities based on an actual metric on the space of surfaces of genus zero, without the need for the selection of landmark points. Our use of conformal maps is taking advantage of a tool to reduce the dimension of the space of correspondences down to a six-dimensional subspace which retains geometric information and is mathematically natural. Its implementation within the program MatchSurface is based on fast and robust numerical methods, making surface comparisons feasible for a wide range of datasets. We have illustrated its use in the field of geometric morphometry, using three datasets representing bones and teeth of primates. Experiments on these datasets show that it performs remarkably well both in shape recognition and in identifying evolutionary patterns.

While we show successful taxon recognition based on geometric information for one of the datasets considered (the Metatarsal dataset, see figure 5), taxonomy is not the intended purpose of this method. Instead, we restrict its current applications to providing robust estimates of the distances between three-dimensional shapes, with one finality being to support phylogeny reconstruction. Since the advent of computers and the developments of robust and fast scientific computing techniques to quantify phenotypes, there has been a wealth of studies attempting to provide a quantitative view of evolution in biology, starting with classification and taxonomy. The concept of numerical taxonomy [48] and the development of three-dimensional geometric morphometrics are both part of this movement (for an excellent review on
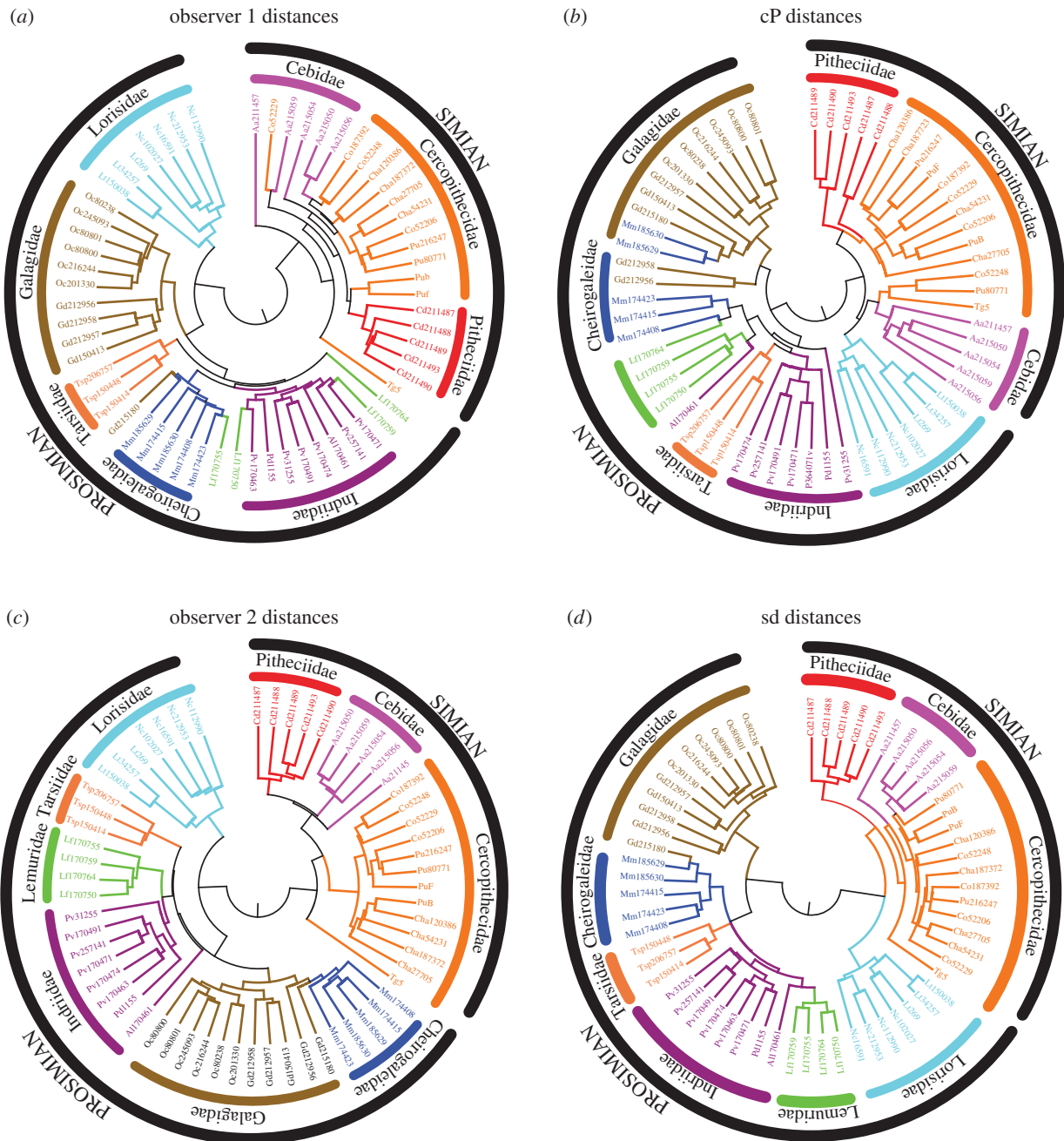
Figure 5. Morphology-based UPGMA trees for the specimens included in the first metatarsal database: (a,c) are derived from distances computed using landmarks placed on each surface by experienced morphometricians, while (b,d) are computed based on landmark-free shape comparison methods, namely cP [13] and sd (this work). Branches of the trees are coloured according to the actual species of the specimens. The trees were computed using the program Neighbor from the software package PHYLIP [45], and subsequently drawn using the package MEGA6 [46].

this topic, see the recent paper by Boyer *et al.* [14]). The development of genomics, however, in the last three decades has led many to question the relevance of geometric morphometrics for phylogenetic studies. Indeed, the assessments of genetic variations from automated genomic analyses have greatly improved our understanding of the relationships between the genotype and phenotype of individuals of many species (for a review, see [49]). Those relationships serve as the basis for building the phylogeny of organisms, i.e. the history of their lineages as they change through time. As a consequence, phylogenetics is playing a central role in the study of evolution [50]. In comparison, it is much harder to develop good models of the genetics that underlie morphological changes [51]. It should be noted also that genomics studies are comparatively easier than morphometric studies, with the cost of sequencing whole genomes being so low today, and with the analyses of the one-dimensional information contained in a genome being significantly simpler than the analyses of the three-dimensional information contained in a shape. As a consequence, the utility of morphological data in phylogenetic research has become increasingly questioned (see, for example, Wiens [11], a comment to a paper by Scotland *et al.* [15]). As a response to the criticisms expressed against geometric morphometry, MacLeod *et al.* [18] and more recently Boyer *et al.* [14] have emphasized the need to automate and standardize morphological studies, starting with the determination of geometric correspondence between shapes. The method developed in this paper is one contribution towards this goal. We have shown that it is robust and versatile, albeit currently limited to studying shapes with surfaces of genus zero.

The method described here extends earlier work presented in [39,40]. The earlier work used energies that did not lead to a metric on the space of shapes. We note that these approaches are most accurate on surfaces that have uniform geometry, without long protrusions or spikes [39]. The method is constrained to finding a conformal map between two surfaces, and, while always possible for genus zero, this cannot in general be done for surfaces of positive genus. The basic idea behind using conformal parametrization for surface mapping is deceptively simple and ultimately very powerful. As genus zero surfaces can always be mapped conformally onto the sphere, the search for (near) isometries between them can be made more tractable by restricting to a search within the Möbius group, which is parametrized with six degrees of freedom only. Spheres can be formed from topological discs by coning their boundaries to their centre of mass. Thus, a method for comparing genus zero surfaces, such as MatchSurface, also gives a method to compare surfaces having the topology of a disc.

Finally, we note that the symmetric deformation energy of a conformal map between two surfaces F_1 and F_2 defined in equation (2.1) establishes a metric on the space of genus zero surfaces. This property is highly desirable for surface comparison, as such a metric is robust and not overly sensitive to noise and measurement errors. The applications of our method extend beyond comparing anatomical surfaces with fields as varied as motion capture, medical imaging and computational biology.

References

1. Angenent S, Pichon E, Tannenbaum A. 2006 Mathematical methods in medical image processing. *Bull. Am. Math. Soc.* **43**, 365–396. (doi:10.1090/S0273-0979-06-01104-9)

2. Zelditch ML, Swiderski DL, Sheets HD. 2012 *Geometric morphometrics for biologists: a primer.* London, UK: Elsevier.

3. Max N, Getzoff E. 1988 Spherical harmonic molecular surfaces. *IEEE Comput. Graph. Appl.* **8**, 42–50. (doi:10.1109/38.7748)

4. Koehl P. 2006 Protein structure classification. In *Reviews in computational chemistry*, vol. 22 (eds KB Lipkowitz, TR Cundari, VJ Gillet, B Boyd), pp. 1–56. Hoboken, NJ: John Wiley & Sons.

5. Kolodny R, Petrey D, Honig B. 2006 Protein structure comparison: implications for the nature of fold space, and structure and function prediction. *Curr. Opin. Struct. Biol.* **16**, 393–398. (doi:10.1016/j.sbi.2006.04.007)

6. Kötter R, Wanke E. 2005 Mapping brains without coordinates. *Phil. Trans. R. Soc. B* **360**, 751–766. (doi:10.1098/rstb.2005.1625)

7. Otte A, Halsband U. 2006 Brain imaging tools in neurosciences. *J. Physiol. Paris* **99**, 281–292. (doi:10.1016/j.jphysparis.2006.03.011)

8. Gholipour A, Kehtarnavaz N, Briggs R, Devous M, Gonipath K. 2007 Brain functional localization: a survey of image registration techniques. *IEEE Trans. Med. Imaging* **26**, 427–451. (doi:10.1109/TMI.2007.892508)

9. MacKenzie-Graham A, Boline J, Toga AW. 2007 Brain atlases and neuroanatomic imaging. *Methods Mol. Biol.* **401**, 183–194. (doi:10.1007/978-1-59745-520-6_11)

10. Pantazis D, Joshi A, Jiang J, Shattuck D, Bernstein LE, Damasio H, Leahy RM. 2010 Comparison of landmark based and automatic methods for cortical surface registration. *Neuroimage* **49**, 2479–2493. (doi:10.1016/j.neuroimage.2009.09.027)

11. Wiens JJ. 2004 The role of morphological data in phylogeny reconstruction. *Syst. Biol.* **53**, 653–661. (doi:10.1080/10635150490472959)

12. Adams DC, Rohlf FJ, Slice DE. 2004 Geometric morphometrics: ten years of progress following the revolution. *Ital. J. Zool.* **71**, 5–16. (doi:10.1080/11250000409356545)

13. Boyer DM, Lipman Y, StClair E, Puente J, Patel BA, Funkhouser T, Jernvall J, Daubechies I. 2011 Algorithms to automatically quantify the geometric similarity of anatomical surface. *Proc. Natl Acad. Sci. USA* **108**, 18 221–18 226. (doi:10.1073/pnas.1112822108)

14. Boyer DM, Puente J, Gladman JT, Glynn C, Mukherjee S, Yapuncich GS, Daubechies I. 2015 A new fully automated approach for aligning and comparing shapes. *Anat. Rec.* **298**, 249–276. (doi:10.1002/ar.23084)

15. Scotland RW, Olmstead RG, Bennett JR. 2003 Phylogeny reconstruction: the role of morphological data. *Syst. Biol.* **52**, 539–548.

16. Weaver T. 2014 Tracing the paths of modern humans from Africa. *Proc. Natl Acad. Sci. USA* **111**, 7170–7171. (doi:10.1073/pnas.1405852111)

17. Reyes-Centero H, Ghirotto S, Détroit F, Grimaud-Hervé D, Barbujani G, Harvati K. 2014 Genomic and cranial phenotype data support multiple modern human dispersals from Africa and a southern route into Asia. *Proc. Natl Acad. Sci. USA* **111**, 7248–7253. (doi:10.1073/pnas.1323666111)

18. MacLeod N, Benfield M, Culverhouse P. 2010 Time to automate identification. *Nature* **467**, 154–155. (doi:10.1038/467154a)

19. Thompson DW. 1917 *On growth and form.* Cambridge, UK: University Press.

20. Gartus A, Geissler A, Foki T, Tahamtan AR, Pahs G, Barth M, Pinker K, Trattnig S, Beisteiner R. 2007 Comparison of fMRI coregistration results between human experts and software solutions in patients and healthy subjects. *Eur. Radiol.* **17**, 1634–1643. (doi:10.1007/s00330-006-0459-z)

21. Turner WD, Brown RE, Kelliher TP, Tu PH, Taister MA, Miller KW. 2005 A novel method of automated skull registration for forensic facial approximation. *Forensic Sci. Int.* **159**, 149–158. (doi:10.1016/j.forsciint.2004.10.003)

22. Lu H, Nolte L-P, Reyes M. 2012 Interest points location for brain image using landmark-annotated atlas. *Int. J. Imaging Syst. Technol.* **22**, 145–152. (doi:10.1002/ima.22015)

23. Cates J, Meyer M, Fletcher PT, Whiteker R. 2006 Entropy-based particle systems for shape correspondence. In *Proc. 1st MICCAI workshop on Mathematical Foundations of Computational Anatomy: Copenhagen, Denmark, 1 October 2006*, pp. 90–99. Lecture Notes in Computer Science. New York, NY: Springer.

24. Cates J, Fletcher PT, Styner M, Shenton M, Whitaker R. 2007 Shape modeling and analysis with entropy-based particle systems. *Inf. Process. Med. Imaging* **20**, 333–345. (doi:10.1007/978-3-540-73273-0_28)

25. Rustamov RM. 2007 Laplace–Beltrami eigenfunctions for deformation invariant shape representation. In *SGP'07, Proc. of the Symposium on Geometry Processing, Eurographics Association, Barcelona, Spain, 46 July 2007*, pp. 225–233. Aire-la-Ville, Switzerland: Eurographics Association.

26. Sun J, Ovsjanikov M, Guibas L. 2009 A concise and provably informative multi-scale signature based on heat diffusion. In *SGP'09, Proc. of the Symposium on Geometry Processing, Eurographics Association, Berlin, Germany, 15–17 July 2009*, pp. 1383–1392. Aire-la-Ville, Switzerland: Eurographics Association.

27. Sampson PD, Bookstein FL, Sheenan FH, Bolson EL. 1996 Eigenshape analysis of left ventricular outlines from contrast ventriculograms. In *Advances in morphometrics*, vol. 22 (eds LF Marcus, M Corti, A Loy, GJP Naylor, DE Slice), pp. 211–233. New York, NY: Plenum Press.

28. Bookstein FL. 1977 Landmark methods for forms without landmarks: localizing group differences in outline shape. *Med. Image Anal.* **1**, 225–243. (doi:10.1016/S1361-8415(97)85012-8)

29. Gunz P, Mitteroecker P, Bookstein FL. 2006 Semilandmarks in three dimensions. In *Modern morphometrics in physical anthropology* (ed. DE Slice), pp. 73–98. New York, NY: Kluwer Academic/ Plenum Publishers.

30. Perez SI, Bernal V, Gonzalez PN. 2006 Differences between sliding semi-landmark methods in geometric morphometrics, with an application to human craniofacial and dental variation. *J. Anat.* **208**, 769–784. (doi:10.1111/j.1469-7580.2006.00576.x)

31. Mitteroecker P, Gunz P. 2009 Advances in geometric morphometrics. *Evol. Biol.* **36**, 235–247. (doi:10.1007/s11692-009-9055-x)

32. Polly PD, MacLeod N. 2008 Locomotion in fossil carnivora: an application of eigensurface analysis for morphometric comparison of 3D surfaces. *Palaeontol. Electron.* **11**, 13.

33. Bronstein AM, Bronstein MM, Kimmel R. 2006 Generalized multidimensional scaling: a framework for isometry-invariant partial surface matching. *Proc. Natl Acad. Sci. USA* **103**, 1168–1172. (doi:10.1073/pnas.0508601103)

34. Huang Q, Adams B, Wicke M, Guibas L. 2008 Non-rigid registration under isometric deformations. In *SGP'08, Proc. of the Symposium on Geometry Processing, Copenhagen, Denmark, 2–4 July 2008*, pp. 1149–1458. Aire-la-Ville, Switzerland: Eurographics Association.

35. Lasowski R, Tevs A, Seidel H-P, Wand M. 2009 A probabilistic framework for partial intrinsic symmetries in geometric data. In *IEEE Int. Conf. on Computer Vision, Kyoto, Japan, 29 September–2 October 2009*, pp. 963–970. New York, NY: IEEE Publishing.

36. Valliant M, Glaunès J. 2005 Surface matching via currents. *Lect. Notes Comp. Sci.* **3565**, 381–392. (doi:10.1007/11505730_32)

37. McCane B. 2013 Shape variation in outline shapes. *Syst. Biol.* **62**, 134–146. (doi:10.1093/sysbio/sys080)

38. Laga H, Kurtek S, Srivastava A, Miklavcic SJ. 2014 Landmark-free statistical analysis of the shape of plant leaves. *J. Theoret. Biol.* **363**, 41–52. (doi:10.1016/j.jtbi.2014.07.036)

39. Koehl P, Hass J. 2014 Automatic alignment of genus-zero surfaces. *IEEE Trans. Pattern Anal. Mach. Intell.* **36**, 466–478. (doi:10.1109/TPAMI.2013.139)

40. Hass J, Koehl P. 2014 How round is a protein? Exploring protein structures for globularity using conformal mapping. *Front. Mol. Biosci.* **1**, 26. (doi:10.3389/fmolb.2014.00026)

41. Bers L. 1972 Uniformization, moduli, and Kleinian groups. *Bull. London Math. Soc.* **4**, 257–300. (doi:10.1112/blms/4.3. 257)

42. Hass J, Koehl P. 2015 A metric for genus-zero surfaces. (http://arxiv.org/abs/1507.00798)

43. Fawcett T. 2006 An introduction to ROC analysis. *Pattern Recogn. Lett.* **27**, 861–874. (doi:10.1016/j.patrec.2005.10.010)

44. Bowie JU, Lüthy R, Eisenberg D. 1991 A method to identify protein sequences that fold into a known three dimensional structure. *Science* **253**, 164–170. (doi:10.1126/science.1853201)

45. Felsenstein J. 1989 PHYLIP—phylogeny inference package (version 3.2). *Cladistics* **5**, 164–166.

46. Tamura K, Stecher G, Peterson D, Filipski A, Kumar S. 2013 MEGA6: molecular evolutionary genetics analysis version 6.0. *Molec. Biol. Evol.* **30**, 2725–2729. (doi:10.1093/molbev/mst197)

47. Robinson DF, Foulds LR. 1981 Comparison of phylogenetic trees. *Math. Biosci.* **53**, 131–147. (doi:10.1016/0025-5564(81)90043-2)

48. Sokal RR. 1963 The principles and practice of numerical taxonomy. *Taxon* **12**, 190–199. (doi:10.2307/1217562)

49. Houle D, Govindaraju DR, Omholt S. 2010 Phenomics: the next challenge. *Nat. Rev.* **11**, 855–866. (doi:10.1038/nrg2897)

50. Doolittle WF. 1999 Phylogenetic classification and the universal tree. *Science* **284**, 2124–2129. (doi:10.1126/science.284.5423.2124)

51. Wiens JJ. 2000 *Phylogenetic analysis of morphological data*. Washington, DC: Smithsonian Books.